In vivo volumetric imaging of biological dynamics in deep tissue via wavefront engineering

Lingjie Kong,[1] Jianyong Tang,[2] and Meng Cui[1,3,4,5,*]

[1] *School of Electrical and Computer Engineering, Purdue University, West Lafayette, IN 47907, USA*
[2]*Laboratory of Systems Biology, National Institute of Allergy and Infectious Diseases, National Institutes of Health, Bethesda, MD 20892, USA*
[3]*Department of Biological Sciences, Purdue University, West Lafayette, IN 47907, USA*
[4]*Integrated imaging cluster, Purdue University, West Lafayette, IN 47907, USA*
[5]*Bindley bioscience center, Purdue University, West Lafayette, IN 47907, USA*
[*]*mengcui@purdue.edu*

Abstract: Biological systems undergo dynamical changes continuously which span multiple spatial and temporal scales. To study these complex biological dynamics *in vivo*, high-speed volumetric imaging that can work at large imaging depth is highly desired. However, deep tissue imaging suffers from wavefront distortion, resulting in reduced Strehl ratio and image quality. Here we combine the two wavefront engineering methods developed in our lab, namely the optical phase-locked ultrasound lens based volumetric imaging and the iterative multiphoton adaptive compensation technique, and demonstrate *in vivo* volumetric imaging of microglial and mitochondrial dynamics at large depth in mouse brain cortex and lymph node, respectively.

OCIS codes: (110.0113) Imaging through turbid media; (110.1080) Active or adaptive optics; (110.7050) Turbid media; (090.1000) Aberration compensation; (180.0180) Microscopy; (180.2520) Fluorescence microscopy; (170.6900) Three-dimensional microscopy; (100.0118) Imaging ultrafast phenomena.

References and links

1. R. N. Germain, E. A. Robey, and M. D. Cahalan, "A Decade of Imaging Cellular Motility and Interaction Dynamics in the Immune System," Science **336**(6089), 1676–1681 (2012).
2. B. F. Grewe and F. Helmchen, "Optical probing of neuronal ensemble activity," Curr. Opin. Neurobiol. **19**(5), 520–529 (2009).
3. M. B. Ahrens, M. B. Orger, D. N. Robson, J. M. Li, and P. J. Keller, "Whole-brain functional imaging at cellular resolution using light-sheet microscopy," Nat. Methods **10**(5), 413–420 (2013).
4. R. Prevedel, Y.-G. Yoon, M. Hoffmann, N. Pak, G. Wetzstein, S. Kato, T. Schrödel, R. Raskar, M. Zimmer, E. S. Boyden, and A. Vaziri, "Simultaneous whole-animal 3D imaging of neuronal activity using light-field microscopy," Nat. Methods **11**(7), 727–730 (2014).
5. H. Dana, A. Marom, S. Paluch, R. Dvorkin, I. Brosh, and S. Shoham, "Hybrid multiphoton volumetric functional imaging of large-scale bioengineered neuronal networks," Nat. Commun. **5**, 3997 (2014).
6. T. Schrödel, R. Prevedel, K. Aumayr, M. Zimmer, and A. Vaziri, "Brain-wide 3D imaging of neuronal activity in Caenorhabditis elegans with sculpted light," Nat. Methods **10**(10), 1013–1020 (2013).
7. M. B. Bouchard, V. Voleti, C. S. Mendes, C. Lacefield, W. B. Grueber, R. S. Mann, R. M. Bruno, and E. M. C. Hillman, "Swept confocally-aligned planar excitation (SCAPE) microscopy for high speed volumetric imaging of behaving organisms," Nat. Photonics **9**(2), 113–119 (2015).
8. R. Yasuda, E. A. Nimchinsky, V. Scheuss, T. A. Pologruto, T. G. Oertner, B. L. Sabatini, and K. Svoboda, "Imaging calcium concentration dynamics in small neuronal compartments," Sci. STKE **2004**(219), pl5 (2004).
9. W. Denk, J. H. Strickler, and W. W. Webb, "Two-photon laser scanning fluorescence microscopy," Science **248**(4951), 73–76 (1990).
10. F. Helmchen and W. Denk, "Deep tissue two-photon microscopy," Nat. Methods **2**(12), 932–940 (2005).
11. K. Svoboda and R. Yasuda, "Principles of two-photon excitation microscopy and its applications to neuroscience," Neuron **50**(6), 823–839 (2006).
12. B. N. G. Giepmans, S. R. Adams, M. H. Ellisman, and R. Y. Tsien, "The fluorescent toolbox for assessing protein location and function," Science **312**(5771), 217–224 (2006).

#253898 Received 13 Nov 2015; revised 25 Dec 2015; accepted 25 Dec 2015; published 14 Jan 2016

13. T.-W. Chen, T. J. Wardill, Y. Sun, S. R. Pulver, S. L. Renninger, A. Baohan, E. R. Schreiter, R. A. Kerr, M. B. Orger, V. Jayaraman, L. L. Looger, K. Svoboda, and D. S. Kim, "Ultrasensitive fluorescent proteins for imaging neuronal activity," Nature **499**(7458), 295–300 (2013).
14. E. J. Botcherby, C. W. Smith, M. M. Kohl, D. Débarre, M. J. Booth, R. Juškaitis, O. Paulsen, and T. Wilson, "Aberration-free three-dimensional multiphoton imaging of neuronal activity at kHz rates," Proc. Natl. Acad. Sci. U.S.A. **109**(8), 2919–2924 (2012).
15. G. Katona, G. Szalay, P. Maák, A. Kaszás, M. Veress, D. Hillier, B. Chiovini, E. S. Vizi, B. Roska, and B. Rózsa, "Fast two-photon in vivo imaging with three-dimensional random-access scanning in large tissue volumes," Nat. Methods **9**(2), 201–208 (2012).
16. L. Kong, J. Tang, J. P. Little, Y. Yu, T. Lämmermann, C. P. Lin, R. N. Germain, and M. Cui, "Continuous volumetric imaging via an optical phase-locked ultrasound lens," Nat. Methods **12**(8), 759–762 (2015).
17. L. Kong and M. Cui, "In vivo Deep Tissue Imaging via Iterative Multi-photon Adaptive Compensation Technique," IEEE J. Sel. Top. Quantum Electron. (2015), in press.
18. M. J. Booth, "Adaptive optical microscopy: the ongoing quest for a perfect image," Light Sci. Appl. **3**(4), e165 (2014).
19. I. M. Vellekoop, "Feedback-based wavefront shaping," Opt. Express **23**(9), 12189–12206 (2015).
20. X. Tao, Z. Dean, C. Chien, O. Azucena, D. Bodington, and J. Kubby, "Shack-Hartmann wavefront sensing using interferometric focusing of light onto guide-stars," Opt. Express **21**(25), 31282–31292 (2013).
21. M. Rueckel, J. A. Mack-Bucher, and W. Denk, "Adaptive wavefront correction in two-photon microscopy using coherence-gated wavefront sensing," Proc. Natl. Acad. Sci. U.S.A. **103**(46), 17137–17142 (2006).
22. D. Débarre, E. J. Botcherby, T. Watanabe, S. Srinivas, M. J. Booth, and T. Wilson, "Image-based adaptive optics for two-photon microscopy," Opt. Lett. **34**(16), 2495–2497 (2009).
23. N. Ji, D. E. Milkie, and E. Betzig, "Adaptive optics via pupil segmentation for high-resolution imaging in biological tissues," Nat. Methods **7**(2), 141–147 (2010).
24. J. Tang, R. N. Germain, and M. Cui, "Superpenetration optical microscopy by iterative multiphoton adaptive compensation technique," Proc. Natl. Acad. Sci. U.S.A. **109**(22), 8434–8439 (2012).
25. L. Kong and M. Cui, "In vivo fluorescence microscopy via iterative multi-photon adaptive compensation technique," Opt. Express **22**(20), 23786–23794 (2014).
26. L. Kong and M. Cui, "In vivo neuroimaging through the highly scattering tissue via iterative multi-photon adaptive compensation technique," Opt. Express **23**(5), 6145–6150 (2015).
27. Z. Kam, P. Kner, D. Agard, and J. W. Sedat, "Modelling the application of adaptive optics to wide-field microscope live imaging," J. Microsc. **226**(1), 33–42 (2007).
28. O. Albert, L. Sherman, G. Mourou, T. B. Norris, and G. Vdovin, "Smart microscope: an adaptive optics learning system for aberration correction in multiphoton confocal microscopy," Opt. Lett. **25**(1), 52–54 (2000).
29. P. S. Tsai, B. Migliori, K. Campbell, T. N. Kim, Z. Kam, A. Groisman, and D. Kleinfeld, "Spherical aberration correction in nonlinear microscopy and optical ablation using a transparent deformable membrane," Appl. Phys. Lett. **91**(19), 191102 (2007).
30. Y. Zhang, S. Poonja, and A. Roorda, "MEMS-based adaptive optics scanning laser ophthalmoscopy," Opt. Lett. **31**(9), 1268–1270 (2006).
31. N. Doble, G. Yoon, L. Chen, P. Bierden, B. Singer, S. Olivier, and D. R. Williams, "Use of a microelectromechanical mirror for adaptive optics in the human eye," Opt. Lett. **27**(17), 1537–1539 (2002).
32. P. Marsh, D. Burns, and J. Girkin, "Practical implementation of adaptive optics in multiphoton microscopy," Opt. Express **11**(10), 1123–1130 (2003).
33. S. G. Adie, B. W. Graf, A. Ahmad, P. S. Carney, and S. A. Boppart, "Computational adaptive optics for broadband optical interferometric tomography of biological tissue," Proc. Natl. Acad. Sci. U.S.A. **109**(19), 7175–7180 (2012).
34. B. Thomas, A. Wolstenholme, S. N. Chaudhari, E. T. Kipreos, and P. Kner, "Enhanced resolution through thick tissue with structured illumination and adaptive optics," J. Biomed. Opt. **20**(2), 026006 (2015).
35. M. Duocastella, G. Vicidomini, and A. Diaspro, "Simultaneous multiplane confocal microscopy using acoustic tunable lenses," Opt. Express **22**(16), 19293–19301 (2014).
36. M. Cui, "Parallel wavefront optimization method for focusing light through random scattering media," Opt. Lett. **36**(6), 870–872 (2011).
37. W. B. Bridges, P. T. Brunner, S. P. Lazzara, T. A. Nussmeier, T. R. O'Meara, J. A. Sanguinet, and W. P. Brown, Jr., "Coherent optical adaptive techniques," Appl. Opt. **13**(2), 291–300 (1974).
38. T. W. Wu, J. Tang, B. Hajj, and M. Cui, "Phase resolved interferometric spectral modulation (PRISM) for ultrafast pulse measurement and compression," Opt. Express **19**(14), 12961–12968 (2011).
39. R. Fiolka, K. Si, and M. Cui, "Complex wavefront corrections for deep tissue focusing using low coherence backscattered light," Opt. Express **20**(15), 16532–16543 (2012).
40. J. H. Park, W. Sun, and M. Cui, "High-resolution in vivo imaging of mouse brain through the intact skull," Proc. Natl. Acad. Sci. U.S.A. **112**(30), 9236–9241 (2015).
41. A. Nimmerjahn, F. Kirchhoff, and F. Helmchen, "Resting microglial cells are highly dynamic surveillants of brain parenchyma in vivo," Science **308**(5726), 1314–1318 (2005).
42. M. Karbowski and R. J. Youle, "Dynamics of mitochondrial morphology in healthy cells and during apoptosis," Cell Death Differ. **10**(8), 870–880 (2003).

#253898 Received 13 Nov 2015; revised 25 Dec 2015; accepted 25 Dec 2015; published 14 Jan 2016

43. J. Mertz, H. Paudel, and T. G. Bifano, "Field of view advantage of conjugate adaptive optics in microscopy applications," Appl. Opt. **54**(11), 3498–3506 (2015).
44. H. P. Paudel, J. Taranto, J. Mertz, and T. Bifano, "Axial range of conjugate adaptive optics in two-photon microscopy," Opt. Express **23**(16), 20849–20857 (2015).
45. T. W. Wu and M. Cui, "Numerical study of multi-conjugate large area wavefront correction for deep tissue microscopy," Opt. Express **23**(6), 7463–7470 (2015).
46. R. D. Simmonds and M. J. Booth, "Modelling of multi-conjugate adaptive optics for spatially variant aberrations in microscopy," J. Opt. **15**(9), 094010 (2013).
47. N. G. Horton, K. Wang, D. Kobat, C. G. Clark, F. W. Wise, C. B. Schaffer, and C. Xu, "In vivo three-photon microscopy of subcortical structures within an intact mouse brain," Nat. Photonics **7**(3), 205–209 (2013).

1. Introduction

The hallmark of life is its dynamics [1, 2]. To study the orchestrated cellular signaling and intercellular interplays *in vivo*, one needs 3D imaging methods that can sample near the natural spatiotemporal resolutions. So far, several wide-field fluorescence imaging methods, such as light-sheet microscopy [3], light-field microscopy [4], and temporal focusing multiphoton microscopy [5, 6], have been developed towards such a goal. The parallel detection scheme of these methods benefits high-speed imaging. However, it only works well for transparent biological systems [7], such as cultured cells, *C Elegans* and zebrafish larvae. In turbid tissue, such as mouse brain and lymph node, the optical aberrations and scattering induce cross-talk in wide-field recording methods and limit the imaging depth. Although image computation and processing can potentially separate the signal sources, the additional photon noise (shot noise) due to the signal crosstalk cannot be removed, which can dramatically reduce the achievable signal-to-noise ratio (SNR). As many of the important applications of optical microscopy such as the calcium imaging demands high SNR [8], spatially parallel detection methods are fundamentally limited in imaging depth.

Currently, laser scanning two-photon microscopy (TPM) remains the method of choice for *in vivo* deep tissue imaging [9–11], in which different spatial points are excited and recorded in series to avoid cross-talk. As the fluorescence excitation is well confined, laser scanning TPM allows the collection of both ballistic and scattered fluorescence emission to represent the signal of the focal point. In comparison, only ballistic fluorescence signal contributes to the correct image and the scattered fluorescence signal generates crosstalk and contaminates SNR in wide field recording. Therefore the fluorescence signal usage efficiency decays exponentially as a function of depth in wide-field recording based methods while laser scanning TPM enjoys excellent signal usage efficiency even at great imaging depth. Overall, the near infrared nonlinear laser excitation and the efficient usage of fluorescence emission contribute to the greatly improved imaging depth of TPM. However, the cost of this imaging depth advantage is the slower imaging speed than that of wide-field recording methods. Advances in brighter fluorophores [12], more sensitive functional indicators [13], and photodetectors of higher quantum efficiency keep improving the two-photon signal. Given that the signal is sufficient, the imaging speed of TPM is limited by the volumetric scanning methods. In conventional TPMs, the inertia of the beam steering hardware sets the bottleneck of scanning speed (the fastest scanning along any dimension is ~10 kHz so far [14]). Meanwhile, the optimized trajectory based scanning methods, such as random access microscopy, are susceptible to motion artifacts [15]. Recently, we have reported a high-speed volumetric imaging system based on optical phase-locked ultrasound lens (OPLUL), where the microsecond scale axial scanning is achieved by conjugating the oscillating defocusing wavefront generated by OPLUL to the pupil plane of the objective lens [16]. We have applied this system in calcium imaging of neuron network activity in the cerebral cortex of behaving mice, and transient morphology imaging of immune cells.

Although the imaging depth of TPM is much improved compared to that of wide-field recording methods, TPM is still susceptible to focus distortion in turbid tissue. The wavefront distortion induced by the inhomogeneous refractive index distribution will not only decrease the resolution, but also limit the achievable SNR and penetration depth. Adaptive optics has

#253898 Received 13 Nov 2015; revised 25 Dec 2015; accepted 25 Dec 2015; published 14 Jan 2016

been applied to microscopy to compensate wavefront distortion for deep tissue imaging [17–34]. Multiple methods of wavefront measurement and compensation have been successfully demonstrated, such as direct wavefront sensing with a wavefront sensor [20] or a low coherence interferometer [21], feedback-based modal wavefront sensing [22] and pupil-segmentation based adaptive optics [23], *etc*. We have developed the iterative multiphoton adaptive compensation technique (IMPACT) [24], and demonstrated its capability in imaging through highly scattering tissue, such as the intact mouse skull [25, 26].

Here we combine the two wavefront engineering techniques, namely OPLUL based volumetric imaging technique and IMPACT, for volumetric imaging of biological dynamics in deep tissue. We show transient morphologies of microglia and mitochondrial network in mouse brain cortex and popliteal lymph node, respectively.

2. Experimental setup and principles

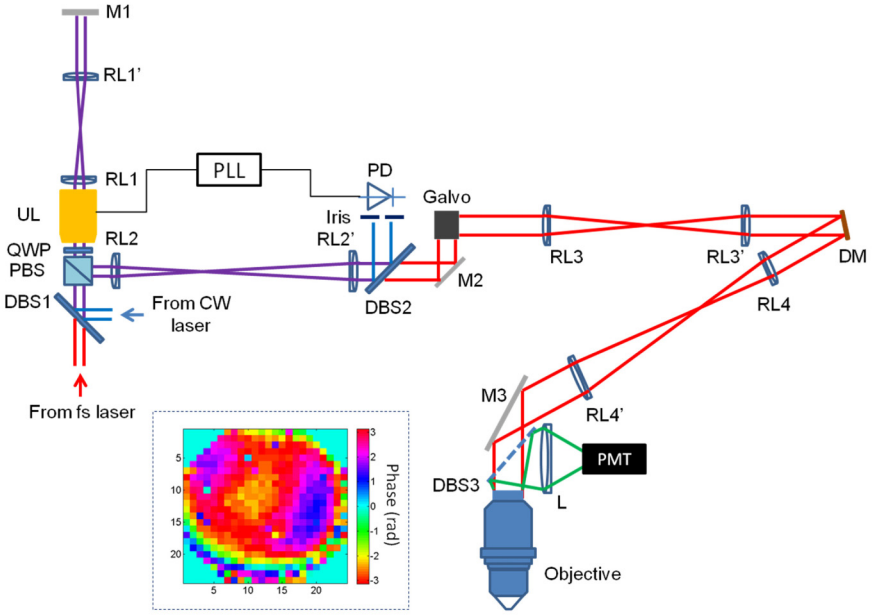

Fig. 1. Diagram of the experimental setup. DBS: dichroic beam splitter, PBS: polarization beam splitter, QWP: quarter wave plate, UL: ultrasound lens, RL: relay lens, M: mirror, PLL: phase-lock loop, PD: photodetector, DM: deformable mirror, L: lens, PMT: photomultiplier tube. The inset: phase pattern for correcting the system aberration.

The experimental setup is shown in Fig. 1. We integrated the OPLUL into an IMPACT based two-photon microscope. The femtosecond (fs) beam (80 MHz, 140 fs, Chameleon, Coherent) and the continuous wave (CW) beam, both of horizontal polarization, were combined by a dichroic beam splitter (DBS1). After going through the polarization beam splitter (PBS), quarter wave plate (QWP) and ultrasound lens (UL, TAG lens 2.0, TAG Optics), the beams were imaged onto the end mirror (M1) by a pair of relay lens (RL1 and RL1'). The reflected beams from M1 went through the UL and QWP again, and were reflected by the PBS. The second pair of relay lens (RL2 and RL2') was used to image the beam onto the galvo scanner. The beams were split by DBS2, with the CW beam reflected onto the photodiode (PD) and the fs beam transmitted through for multiphoton excitation. The CW beam was spatially filtered by an iris before entering the PD whose signal was used as the feedback for the phase-lock loop (PLL, HF2LI-PLL, Zurich Instruments). The fs beam was imaged onto a segmented MEMS deformable mirror (DM, Boston Micromachines Corporations, MA, USA) and the rear pupil plane of the objective (Nikon 16X, NA0.8) sequentially, by the lens pairs of RL3

#253898 Received 13 Nov 2015; revised 25 Dec 2015; accepted 25 Dec 2015; published 14 Jan 2016

and RL3′, RL4 and RL4’ respectively. The emitted fluorescence was collected and detected by a photomultiplier tube (PMT).

We used the UL and DM as the elements for wavefront engineering. They were for generating oscillating defocusing wavefront thus for fast axial scanning [16, 35] and compensating wavefront distortions [24, 36], respectively. In practice, the resonance of the UL may drift resulting from laser heating or fluctuations of environment temperature. To monitor and track the oscillating defocusing wavefront generated by the UL, we introduced the CW beam as the reference. We used the detected signal of the spatially-filtered CW beam by the PD as the input of the PLL to track the drift of the UL resonance, and as the reference signal to reconstruct the images. With the OPLUL, both the amplitude and the phase (with respect to the driving signal) of the UL oscillation were stable, which ensured precise image reconstruction. In addition, we used a double pass configuration to double the axial scan range, as shown in Fig. 1. For high-speed wavefront measurement and compensation, we developed the IMPACT based on the multidither coherent optical adaptive technique [37]. The essence of IMPACT is the iterative parallel wavefront optimization [36, 38, 39] assisted by nonlinearity. We used a segmented DM for phase modulation, and achieved 8 kHz update rate using a Windows workstation. We split the pixels into two groups randomly and uniformly over the available numerical aperture, and took turns to modulate half of the pixels (each pixel at a unique frequency) and measure the phase values (via Fourier transform of the detected signal) while keeping the other half static. This parallel wavefront optimization ensures both high-speed measurement and efficient usage of the fluorescence signal, which are critical for *in vivo* imaging applications. We applied the measured phase values (sign reversed) for wavefront compensation. We also took advantage of the nonlinearity inherent in the multiphoton signals and applied iterative feedback to achieve diffraction limited focus in scattering tissue. It took ~2.4 s for 3 iterations to get the compensation wavefront with a DM of 492 pixels, which is faster than many other sensorless adaptive optics methods. The high-speed operation is required in functional imaging with awake animals and the structural imaging of cellular dynamics, where the motion of the objectives-of-interest may introduce measurement artifacts. As we have demonstrated before [24–26, 40], IMPACT works well in the ballistic regime for *in vivo* imaging, and the compensation wavefront can be effective for >60 minutes when imaging mouse cerebral cortex [17]. Further details of the two techniques can be found in our previous work [16, 24].

In practical imaging, we first performed IMPACT measurements on targets of interest to correct aberrations, and then employed OPLUL for volumetric imaging. We flexibly set the axial scan range by adjusting the amplitude of the voltage signal applied to the UL. The effective volume of the wavefront compensation depends on the complexity of wavefront distortions in the tissue. In the experiments reported here, the axial scan range of OPLUL was 40 μm, within which a single static wavefront correction was sufficient to cover the entire axial scan range. We drove the OPLUL on resonance at ~450 kHz, which enabled microsecond scale axial scanning and was much faster than the galvo based transverse scanning. The voxel rate of the volumetric imaging was ~40 MHz.

3. Experimental results

All procedures involving mice were approved by the Animal Care and Use Committees of Purdue University, HHMI Janelia Research Campus and National Institute of Allergy and Infectious Diseases, National Institutes of Health.

(1) Volumetric imaging of transient morphology of microglia in the mouse brain cortex at large imaging depth

#253898 Received 13 Nov 2015; revised 25 Dec 2015; accepted 25 Dec 2015; published 14 Jan 2016

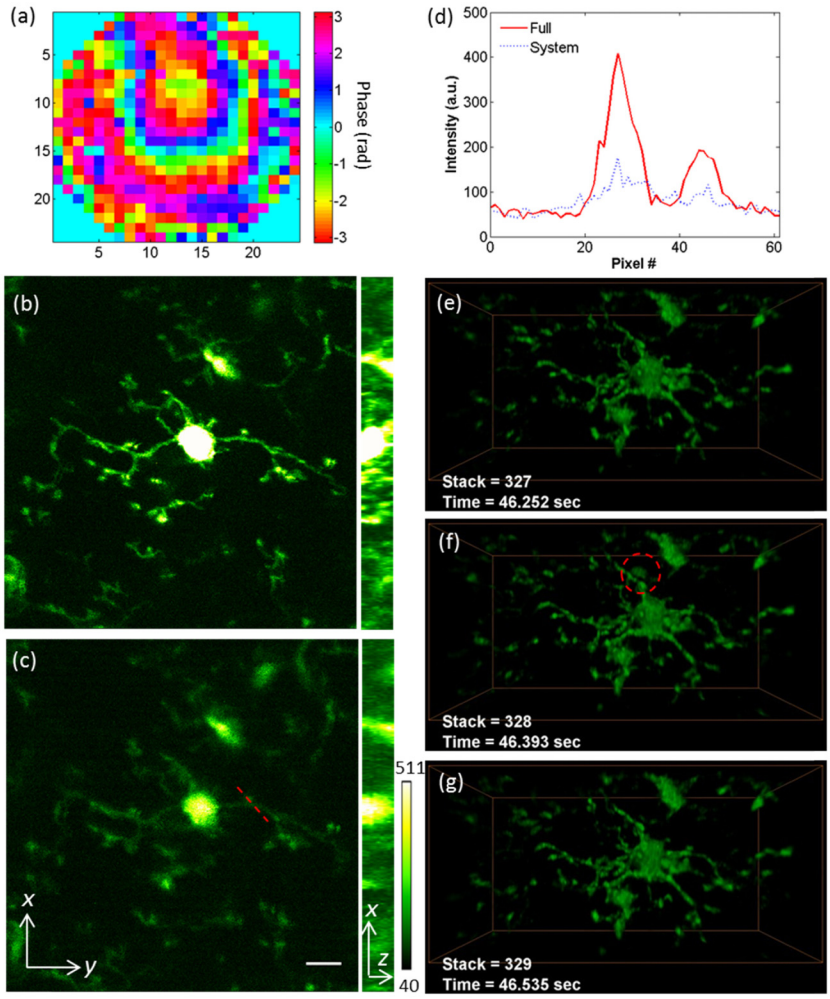

Fig. 2. Volumetric imaging of transient morphology of microglia in mouse brain cortex. (a) The phase pattern for full correction of both system and tissue induced wavefront distortions. (b, c) The maximum intensity projections of the microglia at depth 405-413 μm, with full correction and system correction respectively (Visualization 1). Scale bar: 10 μm. Power: 36 mW at 935 nm. (d) The signal intensity along the dashed line labeled in (c). (e-g) The transient morphologies of the microglia (Visualization 2) at depth 380-420 μm under the dura. Volume size: 98 × 49 × 40 μm^3. The dashed circle in (f) labels a GFP-expressing cell patrolling around the brain cortex through a blood vessel. Laser power: 108 mW at 935 nm.

Microglia are the primary resident immune cells in the central nervous system. Under physiological conditions, the microglia are in the 'resting' state, while their ramified processes continuously extend to and retract from surrounding neural tissues [41]. For monitoring the transient morphology of microglia, we used the Cx3cr1$^{GFP/GFP}$ transgenic mice, and mounted optical windows above the S1 cortex after the craniotomies. We performed IMPACT measurements at 400 μm depth under the dura, and applied the compensation phase pattern to correct both the system and the sample induced aberrations (full correction), as shown in Fig. 2(a). The wavefront contains slight defocusing, which can shift the imaging volume in the axial direction. To avoid the defocusing introduced artifacts in the signal comparisons, shown in Figs. 2(b) and 2(c), we compare the maximum intensity projections of the volume (at depth 405-413 μm under the dura, see Visualization 1) with full correction and system correction, respectively. We also compare the intensities [Fig. 2(d)]

#253898 Received 13 Nov 2015; revised 25 Dec 2015; accepted 25 Dec 2015; published 14 Jan 2016

along the dashed line in Fig. 2(c). As reported before, with the help of IMPACT, the signal was much improved while the background fluorescence kept the same level [24–26]. Maintaining the full correction pattern on the DM, we then employed OPLUL for volumetric imaging. We imaged the dynamics in a volume of 98 × 49 × 40 μm^3 at the depth of 380-420 μm under the dura at 7 Hz, during which we switched the compensation wavefront patterns between full correction and system correction to show the effectiveness of our methods (Visualization 2). The fast volumetric imaging also enabled us to capture rare events. In addition to microglia, some leukocytes circulating in the vasculature of the $Cx3cr1^{GFP/GFP}$ mice also express GFP [16]. In Figs. 2(e)-2(g), we show the snapshot of one GFP-expressing cell (likely a monocyte, or NK cell) patrolling through the imaging volume.

(2) Volumetric imaging of the dynamics of mitochondrial network in lymphocytes of mouse lymph node

Mitochondria form dynamical networks during cellular metabolism, whose subcellular distribution and morphology can change continually [42]. The imaging of mitochondrial dynamics is essential to reveal its crucial roles in physiology and pathology. We collected mito-Dendra2 expressing lymphocytes from the spleen of the $PhAM^{excised}$ transgenic mice, and transferred ~100 μL of the diluted cellular solution into the circulation system of the wild-type mice via tail-vein injections. After ~2 hours, we surgically exposed the popliteal lymph node of the wild-type mice, and imaged the dynamics of the mitochondrial networks in the lymphocytes. In Fig. 3(a), we show the phase pattern for full correction, measured at 347 μm depth under the surface. The volume view (17.6 × 17.6 × 18 μm^3) with this full correction is shown in Fig. 3(b), and the same volume imaged with system correction is shown in Fig. 3(c). In Figs. 3(d)-3(f), we extract one plane from the volume and show the signal improvement quantitatively. We performed volumetric imaging of the dynamical mitochondrial networks (at depth 340-364 μm, 3.5 Hz). It is worth noting that the mitochondrial dynamics can be recorded even when there was substantial respiration induced motion (Visualization 3). Several snapshots of the mitochondria network in a lymphocyte cell are shown in Figs. 3(g)-3(i), which was undergoing continuous change.

4. Discussion and conclusions

As shown in these *in vivo* imaging applications, IMPACT worked well for compensating wavefront distortions in live animals. Compared with other adaptive optics methods, it features high-speed operation and high-order wavefront correction [17]. High-speed operation allows awake animal and cellular dynamics imaging, where the objectives-of-interest are under constant motion. High-order wavefront correction (up to 492 spatial modes in current implementations) allows us to image through highly scattering tissue. However, due to the heterogeneity of biological tissue, the effective compensation volume became smaller at greater imaging depth [17]. Novel development to achieve simultaneous large volume correction is needed. Additionally, the OPLUL induced dynamical aberrations (mainly spherical aberrations) [16], which requires fast dynamic compensation at ~450 kHz. We have proposed to cancel the dynamical aberrations with another UL [16], which however is quite complex. Nevertheless, by combining IMPACT and the OPLUL based volumetric imaging, we can record the dynamics within the compensation volume in 3D with improved signal strength and signal-to-background-ratio, which provides a solution for volumetric imaging of biological dynamics at large depth.

#253898 Received 13 Nov 2015; revised 25 Dec 2015; accepted 25 Dec 2015; published 14 Jan 2016

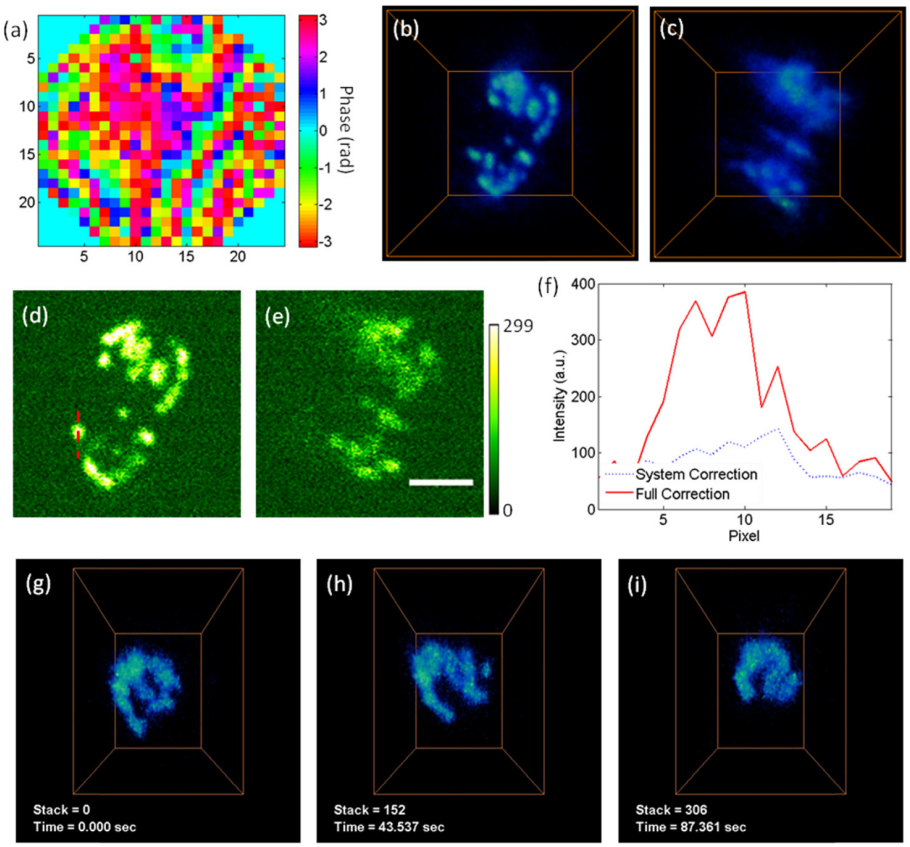

Fig. 3. Volumetric imaging of the dynamics of mitochondrial network in lymphocytes of mouse lymph node. (a) The phase pattern for full correction of both system and tissue induced wavefront distortions. (b, c) The volume views of mitochondria in lymphocytes, with full correction and system correction respectively. The volume is 17.6 × 17.6 × 18 μm^3, at the depth of 340-364 μm under the surface. Laser power: 55 mW at 935 nm. (d, e) The images acquired at 348 μm depth, with full correction and system correction respectively. Scale bar: 5 μm. (f) The signal intensity along the dashed line labeled in (e). (g-i) The transient morphologies of the mitochondria in lymphocytes (Visualization 3). Volume size: 12 × 9 × 18 μm^3. Laser power: 90 mW at 935 nm.

We expect that the deep tissue volumetric imaging demonstrated here can also be implemented by combining OPLUL with other configurations of wavefront correction, such as the single conjugated adaptive optics [40, 43–46] which has shown extended compensation field of view. Moreover, IMPACT and OPLUL are both compatible with fluorophores of longer excitation and emission wavelengths in two-photon and three-photon excitation [47], which can further improve the imaging depth.

In summary, we combine two wavefront engineering techniques for volumetric imaging of biological dynamics in deep tissue, using OPLUL for fast axial scanning and IMPACT for wavefront compensation. We applied this system to *in vivo* volumetric imaging of microglia in mouse brain cortex and mitochondrial network in mouse popliteal lymph node.

Acknowledgments

L.K. and M.C. thank the support from NIH (1U01NS094341-01), Purdue University, and Howard Hughes Medical Institute. This research was also supported in part by the Intramural Research Program of the National Institute of Allergy and Infectious Diseases, National Institutes of Health.

#253898 Received 13 Nov 2015; revised 25 Dec 2015; accepted 25 Dec 2015; published 14 Jan 2016